

Effect of magnetic field on jet transport coefficient \hat{q}

Debjani Banerjee¹, Prottoy Das¹, Souvik Paul², Abhi Modak¹, Ankita Budhraj³, Sabyasachi Ghosh⁴, and Sidharth K. Prasad¹

¹Department of Physics, Bose Institute, EN 80, Sector-V, Salt Lake, Kolkata 700091, West Bengal, India

²Department of Physical Sciences, Indian Institute of Science Education and Research, Kolkata, Mohanpur 741246, West Bengal, India

³Tata Institute of Fundamental Research, Homi Bhabha Road, Colaba, Mumbai 400005, Maharashtra, India

⁴Indian Institute of Technology Bhilai, GEC Campus, Sejbahar, Raipur 492015, Chhattisgarh, India

Abstract

We report the estimation of jet transport coefficient, \hat{q} for quark and gluon initiated jets using a simple quasi-particle model in absence and presence of magnetic field. This model introduces a temperature and magnetic field-dependent degeneracy factor of partons, which is tuned by fitting the entropy density of lattice quantum chromodynamics data. At a finite magnetic field, \hat{q} for quark jets splits into parallel and perpendicular components whose magnetic field dependence comes from two sources: the field-dependent degeneracy factor and the phase space part guided from the shear viscosity to entropy density ratio. Due to the electrically neutral nature of gluons, the estimation of \hat{q} for gluon jets is affected only by the field-dependent degeneracy factor. In presence of a finite magnetic field, we find a significant enhancement in \hat{q} for both quark and gluon initiated jets at low temperature, which gradually decreases towards high temperature. We compare the obtained results with the earlier calculations based on the AdS/CFT correspondence, and a qualitatively similar trend is observed. The change in \hat{q} in presence of magnetic field is, however, quantitatively different for quark and gluon jets. This is an interesting observation which can be explored experimentally to verify the effect of magnetic field on \hat{q} .

1 Introduction

In high energy hadron-hadron, hadron-nucleus and nucleus-nucleus collisions, the partons produced in large-momentum transfer (large Q^2) processes undergo multiple splittings (forming shower of partons) and hadronization, leading to a collimated spray of energetic colorless hadrons known as jets [1]. Jets are produced very early in the collision due to their small formation time [2, 3]. In nucleus-nucleus (AA) collisions, where a thermalized (expanding) medium, quark gluon plasma (QGP) is produced, these jets lose their energy via elastic and inelastic interactions with the medium partons while passing through it, resulting in the suppression of high energy jets in AA collisions relative to that in pp and pA collisions.

This phenomenon of jet energy loss is known as jet quenching [4–7] and can be quantified experimentally by a well-known observable, the nuclear modification factor R_{AA} , defined as the ratio of high momentum inclusive hadron or jet yields in AA collisions to that in N_{coll} (number of binary collisions) scaled pp collisions. Suppression of high-momentum hadrons and jets was previously measured by NA49, PHENIX, CMS and ALICE experiments at SPS, RHIC and LHC [8–12]. Within the framework of theoretical models, jet quenching can be studied to extract and provide constraints on the jet transport coefficient \hat{q} of the QGP, which is defined by the mean square of the momentum transfer between the propagating hard jet and the soft medium per unit path length. The jet initiated by a quark (gluon) is known as quark (gluon) jet. The quark and gluon jets have different sensitivity to the medium due to differences in their color degrees of freedom. The amount of transverse momentum broadening of the jet can be related to density of the gluon distribution in the medium [13, 14]. This allows a temperature-dependent proportional relation between \hat{q} and gluon density.

The phenomena of jet quenching has been very well explored by various theoretical models [7], viz. GLV-CUJET [15–17], MARTINI [18], MCGILL-AMY [19], HT-M [6, 20], HT-BW [21–23], etc. The value of \hat{q} is estimated in these models by explaining the experimentally measured quantity R_{AA} . To encapsulate the parton energy loss, different approaches are used by these models. GLV-CUJET relies on multiple scattering in the medium for energy loss and is controlled by the strong coupling constant, the Debye screening mass and the density of scattering centers. HT-BW, HT-M use high-twist (HT) approach where the energy loss is only affected by \hat{q} . Within the hard-thermal-loop (HTL) resummed thermal field theory-based MARTINI and MCGILL-AMY models, the only controlling parameter for energy loss is the strong coupling constant. Based on R_{AA} for neutral pion spectra reported by PHENIX experiment [24, 25], the extracted values of the jet transport coefficient at the initial time of QGP formation, \hat{q}_0 , are $0.9^{+0.05}_{-0.04}$ GeV²/fm [23] for 0–10% central and 1.2 ± 0.3 GeV²/fm [7] for 0–5% central Au–Au collisions at $\sqrt{s_{NN}} = 0.2$ TeV for $\tau_0 = 0.6$ fm/c. Similarly based on combined ALICE [26] and CMS [27] data on charged hadron spectra in 0–5% central Pb–Pb collisions at $\sqrt{s_{NN}} = 2.76$ TeV, the extracted value of \hat{q}_0 at $\tau_0 = 0.6$ fm/c is 2.2 ± 0.5 GeV²/fm [7].

In non-central nucleus-nucleus collisions, a large magnetic field (B) is expected to be created due to moving charges (spectators) at relativistic energies. The strength of this magnetic field produced immediately after the collision is predicted to reach up to a value of m_π^2 ($\sim 10^{18}$ G) at RHIC and $10m_\pi^2$ at LHC [28]. It is very important to study the effect of this large magnetic field on various QGP properties such as jet transport coefficient, \hat{q} .

This article explores the effect of magnetic field on \hat{q} . Without going into the microscopic calculation, a prescription similar to Ref. [23] is followed where the transition from \hat{q}_0 to \hat{q}_N (jet transport coefficient at the centre of the cold nuclear matter in a large nucleus) and vice-versa are mapped through a quasi-particle type description [29], based on the thermodynamics of lattice quantum chromodynamics (LQCD) [30, 31], to estimate \hat{q} in absence of magnetic field. Later it is extended for a finite magnetic field picture, based on the LQCD magneto-thermodynamical quantities [32, 33]. Similar kind of magnetic field extension of quasi-particle models has been addressed in Refs. [34–37], based on effective QCD models. This approach is not so rich to deal with effective dynamics, but an easy-dealing parameter based model to map LQCD magneto-thermodynamical quantities. To add an anisotropic phase space part, at finite temperature T and magnetic field B , the relation between shear viscosity η and \hat{q} in presence of magnetic field [38–43] is considered.

This article is organized as follows. Sec. 2 describes the mapping of LQCD thermody-

namical quantities in presence of magnetic field by introducing a temperature and magnetic field-dependent degeneracy factor. The formalism to estimate jet transport coefficient using quasi-particle description and the magnetic field-dependent jet transport coefficient using the temperature and magnetic field-dependent phase space part of shear viscosity are discussed in Sec. 3. The results obtained in this work and their comparisons with the AdS/CFT correspondence are presented in Sec. 4. The outcome of this work is summarized in Sec. 5.

2 Parametrization of LQCD magneto-thermodynamical data using quasi-particle model

This section describes the procedure adopted to map LQCD thermodynamical data [33] in presence of magnetic field following the steps outlined in [29]. In terms of the Fermi-Dirac

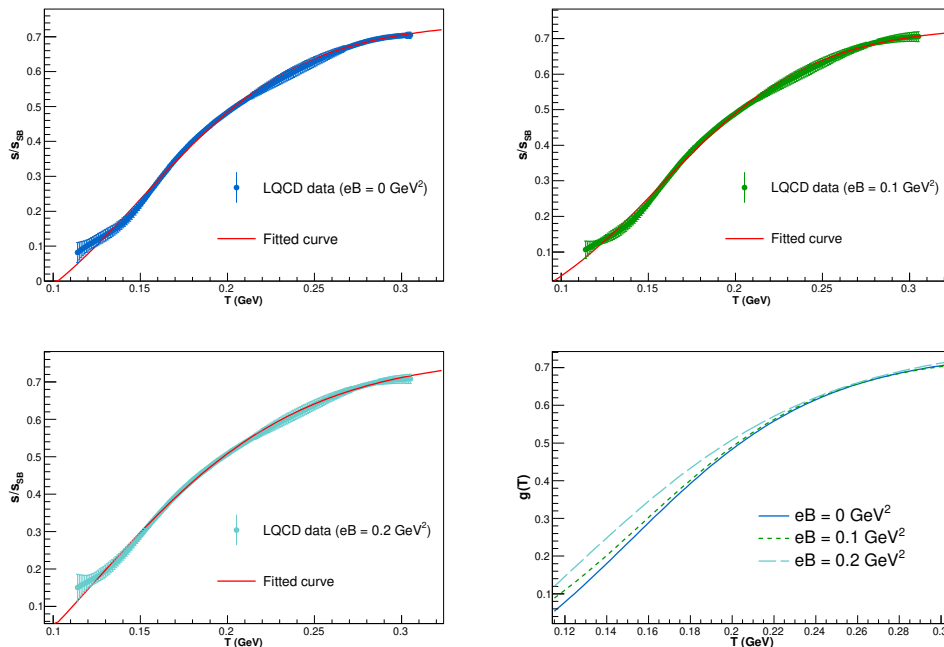


Figure 1: Top left, top right and bottom left: LQCD data points (with error bars) [33] and fitted curves using Eq. (7) (solid line) of normalized entropy density, normalized by its SB limit (s_{SB}) vs T at $eB = 0$ (blue line), $eB = 0.1$ GeV² (green line) and $eB = 0.2$ GeV² (cyan line). Bottom right: Corresponding T -dependent fraction $g(T)$ [Eq. (7)] at different eB (to be multiplied with total degeneracy factor).

(FD) distribution function of quarks and the Bose-Einstein (BE) distribution function of gluons, the energy density (ϵ) and pressure (P) of the QGP system can be expressed as

$$\epsilon_{QGP} = g_g \int_0^\infty \frac{d^3\vec{k}}{(2\pi)^3} \frac{\omega_g}{e^{\beta\omega_g} - 1} + g_Q \int_0^\infty \frac{d^3\vec{k}}{(2\pi)^3} \frac{\omega_Q}{e^{\beta\omega_Q} + 1} \quad (1)$$

and

$$P_{QGP} = g_g \int_0^\infty \frac{d^3 \vec{k}}{(2\pi)^3} \left(\frac{\vec{k}^2}{3\omega_g} \right) \frac{1}{e^{\beta\omega_g} - 1} + g_Q \int_0^\infty \frac{d^3 \vec{k}}{(2\pi)^3} \left(\frac{\vec{k}^2}{3\omega_Q} \right) \frac{1}{e^{\beta\omega_Q} + 1} \quad (2)$$

where ω_Q, ω_g are energies and

$$\begin{aligned} g_Q &= (\text{spin}) \times (\text{particle/antiparticle}) \times (\text{color}) \times (\text{flavor}) \\ &= 2 \times 2 \times 3 \times 3 = 36, \\ g_g &= (\text{spin}) \times (\text{flavor}) = 2 \times 8 = 16, \end{aligned} \quad (3)$$

are degeneracy factors of quarks and gluons respectively. At zero net quark density or chemical potential, the entropy density (s) can be expressed in terms of P and ϵ as

$$s_{QGP} = \frac{P_{QGP} + \epsilon_{QGP}}{T}. \quad (4)$$

For a massless QGP system,

$$\begin{aligned} P_{QGP} &= \left[g_g + g_Q \left(\frac{7}{8} \right) \right] \frac{\pi^2}{90} T^4 \approx 5.2 T^4, \\ \epsilon_{QGP} &= \left[g_g + g_Q \left(\frac{7}{8} \right) \right] \frac{3\pi^2}{90} T^4 \approx 15.6 T^4, \\ s_{QGP} &= \left[g_g + g_Q \left(\frac{7}{8} \right) \right] \frac{4\pi^2}{90} T^3 \approx 20.8 T^3. \end{aligned} \quad (5)$$

Now, if one sees the LQCD data of $P(T), \epsilon(T), s(T)$ at $eB = 0$ from Ref. [33], then one can notice that the data points always remain lower than their massless limits, i.e. $P/T^4 < 5.2, \epsilon/T^4 < 15.6, s/T^4 < 20.8$. A rich QCD interaction in the non-perturbative domain is responsible for this suppression, and it is LQCD calculation that provides useful insights in this domain, where pQCD does not work well. One can map this temperature-dependent suppression of $P(T), \epsilon(T), s(T)$ [29] by imposing a temperature-dependent fraction $g(T)$, multiplied with the total degeneracy factor of QGP. So, this picture assumes that while going from high temperature to low temperature, the degeneracy factor of the massless QGP system is gradually reduced. Instead of considering massless QGP, one can consider physical mass of quark in Eqs. (1), (2) and (4) and then fit their P, ϵ and s with LQCD data by tuning $g(T)$. However, in this work, the massless QGP expression is adopted due to its visibility for simple analytic structure. One should also note that the numerical difference between massless QGP and QGP with physical mass is quite small.

Now, let us proceed with a finite magnetic field picture. The presence of finite magnetic field results in an anisotropy in the pressure. However, if both the magnetic field and the pressure are along z -direction, then the thermodynamic relation

$$s = \frac{\epsilon + P_z}{T} \quad (6)$$

remains the same [32]. Therefore, the earlier expressions can still be used for finite B picture by introducing a T, B -dependent parameter $g(T, B)$. The parametric form of $g(T, B)$ can be obtained by mapping LQCD data of $P(T, B), \epsilon(T, B), s(T, B)$ [32, 33]:

$$g(T, B) = a_0 - \frac{a_1}{e^{a_2(T-0.17)} + a_3}. \quad (7)$$

Exact mapping of all these thermodynamical quantities (P , ϵ , s) simultaneously using a single set of parameters of $g(T, B)$ is very difficult. Therefore, in this work, only the entropy density is chosen because one of the aims is also to estimate s/η later, which is connected with the dimensionless ratio \hat{q}/T^3 . In this context, the mapping used here might not be considered so robust but can surely be considered as a simplified and easy-dealing tool. Figure 1 shows the LQCD data points and their fitted curves of normalized entropy density at $eB = 0, 0.1$ and 0.2 GeV^2 using Eq. (7) and T -dependent fraction $g(T)$ at different eB respectively and the corresponding values of the tuning parameters ($a_{0,1,2,3}$) are summarized in Table 1.

Table 1: Different values of $a_{0,1,2,3}$ given in Eq. (7) for different magnetic field strengths

$eB(\text{GeV}^2)$	\mathbf{a}_0	\mathbf{a}_1	\mathbf{a}_2	\mathbf{a}_3
0.0	-0.26	-1.49	-21.58	1.49
0.1	-0.16	-1.20	-22.61	1.33
0.2	-0.47	-2.82	-16.51	2.26

3 Jet transport coefficient \hat{q}

The temperature-dependent jet transport coefficient $\hat{q}(T)$ of a medium of hadron resonance gas can be approximated, following Ref. [23], as:

$$\hat{q}(T) = \frac{\hat{q}_N}{\rho_N} \rho_h(T), \quad (8)$$

where $\hat{q}_N \approx 0.02 \text{ GeV}^2/\text{fm}$ [44, 45] is the jet transport coefficient at the center of the cold nuclear matter in a large nucleus, $\rho_N = 0.17 \text{ fm}^{-3}$ is nuclear saturation density and ρ_h is hadronic matter density. In Ref. [23], $\rho_h(T)$ is obtained using hadron resonance gas (HRG) model within the hadronic temperature range. The thermodynamics in the HRG model is found to match well with LQCD data in the hadronic temperature range. Here, a quasi-particle model with temperature-dependent degeneracy factor, which is obtained from parameterizing LQCD data as discussed in Sec. 2, has been used as an alternative approach for estimations of thermodynamical quantities and it is not only used for hadronic temperature domain but also for quark temperature domain, beyond the quark-hadron phase transition. Because the jet transport coefficient is expected to be proportional to the effective density of the scatterers in the medium, which is dominated by gluons [13, 23, 39], the hadronic matter density $\rho_h(T)$ can be replaced by the density of gluons in the medium $\rho_G(T)$ and consider it for the entire temperature range.

Similar to Eqs. (1) and (2), the gluon density ρ_G can be expressed as:

$$\rho_G = g_g \int_0^\infty \frac{d^3\vec{k}}{(2\pi)^3} \frac{1}{e^{\beta\omega_g} - 1}. \quad (9)$$

Massless gluons provide analytic expression:

$$\begin{aligned} \rho_G &= \left[g_g \frac{\zeta(3)}{\pi^2} \right] T^3 \\ &= 1.94 T^3, \end{aligned} \quad (10)$$

which can be considered as high temperature ($T \rightarrow \infty$) limiting values, where pQCD works well. Therefore, grossly one can consider it as gluon density in pQCD domain and its corresponding high temperature limiting expression of \hat{q} will be

$$\hat{q}_\infty = \frac{\hat{q}_N}{\rho_N} \times 1.94 T^3 = 3.03 \times 1.94 T^3 \quad (11)$$

whose normalized value \hat{q}_∞/T^3 saturates at 5.87.

In the non-perturbative QCD domain, one can make a rough estimation of the gluon density by multiplying $1.94 T^3$ with the temperature-dependent degeneracy factor $g(T)$. Following Eq. (8) and taking \hat{q}_N as the reference point, the jet transport coefficient $\hat{q}(T)$ for the entire temperature range can be written as:

$$\begin{aligned} \hat{q}(T) &= \frac{\hat{q}_N}{\rho_N} \times g(T) \times g_g \frac{\zeta(3)}{\pi^2} T^3 \\ &= 3.03 \times \left[a_0 - \frac{a_1}{e^{a_2(T-0.17)} + a_3} \right] \times 1.94 T^3 \end{aligned} \quad (12)$$

The above expression is built from the cold nuclear matter reference point and it extends from hadronic to quark temperature domain. As an alternative way, one can make initial value of jet quenching \hat{q}_0 as reference point and extend it from high (quark) to low (hadronic) temperature range. In this case, assuming an equivalence between \hat{q}_0 and \hat{q} one can normalize Eq. (12) by multiplying with \hat{q}_0/\hat{q}_∞ :

$$\begin{aligned} \hat{q}(T) &= \frac{\hat{q}_N}{\rho_N} \times g(T) \times g_g \frac{\zeta(3)}{\pi^2} T^3 \left(\frac{\hat{q}_0}{\hat{q}_\infty} \right) \\ &= g(T) \times \hat{q}_0 \\ &= \left[a_0 - \frac{a_1}{e^{a_2(T-0.17)} + a_3} \right] \times 0.9 \text{ GeV}^2/\text{fm}. \end{aligned} \quad (13)$$

Therefore, either by using Eq. (12) or Eq. (13), one can make an estimation of $\hat{q}(T)$ in the quasi-particle model. The parameters (a_0 , a_1 , a_2 and a_3) of the temperature-dependent degeneracy factor $g(T)$ in the model are obtained by fitting the LQCD data, as discussed in Sec. 2. For the estimation of $\hat{q}(T)$ in absence of magnetic field, the model uses LQCD data at $eB = 0$ to obtain its fit parameters. Through the above two equations, the quasi-particle model also provides a beautiful tool to study the effect of magnetic field on $\hat{q}(T)$. At finite magnetic field, a T - and B -dependent degeneracy factor $g(T, B)$ replaces $g(T)$ in the above equations. The parameters of $g(T, B)$ are obtained by fitting the LQCD magnetothermodynamical data at $eB = 0.2 \text{ GeV}^2$. This extension to finite magnetic field domain has different impacts in the estimation of $\hat{q}(T, B)$ for quark and gluon jets. In case of gluon jets, only the medium gets influenced by the presence of magnetic field, whereas quark jets being electrically charged also experience the effect of magnetic field along with the medium. Similar to other transport coefficients such as shear viscosity, electrical conductivity of QGP, $\hat{q}(T, B)$ can have a multicomponent structure (e.g. \hat{q}_\parallel , \hat{q}_\perp , etc.) for quark jets which are discussed in the next subsection.

3.1 Phase space component of $\hat{q}(T, B)$ for quark jets

According to Refs. [38–42], the jet transport coefficient is connected with the shear viscosity coefficient. Here, $\hat{q}(T, B)$ is calculated from the knowledge of $\eta(T, B)$ profile. The advantage

of this approach lies in the fact that the T , B -dependent phase space part of $\eta(T, B)$ is well studied in Refs. [46–59]. So, based on that knowledge, the T , B -dependent phase space part has been invoked into $\hat{q}(T, B)$.

Let us take a quick revisit of shear viscosity expressions at finite temperature and magnetic field. First, one can consider the case of zero magnetic field and then move to the non-zero magnetic field picture. According to the macroscopic fluid definition, shear viscosity η is the proportionality constant between viscous stress tensor π^{ij} and velocity gradient tensor C^{ij} [59], i.e.

$$\pi^{ij} = \eta C^{ij}, \quad (14)$$

which is relativistic and tensor form of the so-called Newton's law of viscosity. In the microscopic kinetic theory approach, the viscous stress tensor can be connected with the deviation (from the equilibrium distribution function f_0) $\delta f = C k^k k^l C_{kl} \beta f_0 (1 \mp a f_0)$ as

$$\begin{aligned} \pi^{ij} &= g \int \frac{d^3 \vec{k}}{(2\pi)^3} \frac{k^i k^j}{\omega} \delta f \\ &= g \int \frac{d^3 \vec{k}}{(2\pi)^3} \frac{k^i k^j}{\omega} C k^k k^l C_{kl} \beta f_0 (1 - a f_0), \end{aligned} \quad (15)$$

where $f_0 = 1/[e^{\beta\omega} + a]$ denotes the Fermi-Dirac (FD) and Bose-Einstein (BE) distribution functions for $a = \pm 1$ respectively and $\omega = \sqrt{\vec{k}^2 + m^2}$ is the energy of medium constituent with mass m and degeneracy factor g . Connecting the macroscopic Eq. (14) and microscopic Eq. (15), one can get the shear viscosity tensor:

$$\eta^{ijkl} = g \int \frac{d^3 \vec{k}}{(2\pi)^3} \frac{k^i k^j k^k k^l}{\omega^2} \tau_c \beta f_0 (1 - a f_0), \quad (16)$$

whose isotropic expression will be

$$\eta = \frac{g}{15} \int \frac{d^3 \vec{k}}{(2\pi)^3} \frac{\vec{k}^4}{\omega^2} \tau_c \beta f_0 (1 - a f_0). \quad (17)$$

The unknown constant C in Eq. (15) has been obtained in terms of relaxation time τ_c with the help of relaxation time approximation (RTA) based relativistic Boltzmann equation (RBE) [59].

In presence of magnetic field, five independent traceless tensors are proposed in Ref. [46–48] instead of a single traceless velocity gradient tensor C^{ij} . Here, two sets of five shear viscosity components $\tilde{\eta}_{0,1,2,3,4}$ [51, 55, 59] and $\eta_{0,1,2,3,4}$ [57, 59] are obtained, which are interconnected. The two main components based on the direction of the applied magnetic field are as follows:

$$\begin{aligned} \frac{\eta_{\parallel}}{\eta} &= \frac{\tilde{\eta}_2}{\eta} = \frac{(\eta_0 + \eta_2)}{\eta} = \frac{1}{1 + (\tau_c/\tau_B)^2} \\ \frac{\eta_{\perp}}{\eta} &= \frac{\tilde{\eta}_1}{\eta} = \frac{\eta_0}{\eta} = \frac{1}{1 + 4(\tau_c/\tau_B)^2}, \end{aligned} \quad (18)$$

where another time scale $\tau_B = E_{jet}/e_q B$ (E_{jet} is the jet energy) will come into the picture along with relaxation time τ_c . Here, e_q denotes the electric charge of quarks. A simplified

general expression of shear viscosity for massless case is as follows,

$$\begin{aligned}\eta &= \frac{4g \tau_c}{5\pi^2} \zeta(4) T^4 \text{ for BE} \\ &= \left(\frac{7}{8}\right) \frac{4g \tau_c}{5\pi^2} \zeta(4) T^4 \text{ for FD .}\end{aligned}\quad (19)$$

Now, for massless 3 flavor QGP at $B = 0$, one can get

$$\begin{aligned}\eta &= \left[16 + \frac{7}{8}36\right] \frac{4 \tau_c}{5\pi^2} \zeta(4) T^4 , \\ s &= \left[16 + \frac{7}{8}36\right] \frac{4 \tau_c}{\pi^2} \zeta(4) T^3 , \\ \Rightarrow \frac{\eta}{s} &= \frac{\tau_c T}{5} .\end{aligned}\quad (20)$$

For $B \neq 0$, one gets

$$\begin{aligned}\frac{\eta_{\parallel}}{s} &= \frac{1}{\left[16 + \frac{7}{8}36\right]} \left[16 + \frac{7}{8}12 \sum_{u,d,s} \frac{1}{1 + (\tau_c/\tau_B)^2}\right] \frac{\tau_c T}{5} \\ \frac{\eta_{\perp}}{s} &= \frac{1}{\left[16 + \frac{7}{8}36\right]} \left[16 + \frac{7}{8}12 \sum_{u,d,s} \frac{1}{1 + 4(\tau_c/\tau_B)^2}\right] \frac{\tau_c T}{5} .\end{aligned}\quad (21)$$

Now, by roughly connecting $\hat{q} \propto s/\eta$ at $B = 0$ and $\hat{q}_{\parallel,\perp} \propto s/\eta_{\parallel,\perp}$ at $B \neq 0$ one may write:

$$\begin{aligned}\frac{\hat{q}_{\parallel}(B)}{\hat{q}(B=0)} &= \frac{s/\eta_{\parallel}}{s/\eta} = \frac{47.5}{\left[16 + \frac{7}{8}12 \sum_{u,d,s} \frac{1}{1 + (\tau_c/\tau_B)^2}\right]} \\ \frac{\hat{q}_{\perp}(B)}{\hat{q}(B=0)} &= \frac{s/\eta_{\perp}}{s/\eta} = \frac{47.5}{\left[16 + \frac{7}{8}12 \sum_{u,d,s} \frac{1}{1 + 4(\tau_c/\tau_B)^2}\right]} .\end{aligned}\quad (22)$$

Now realizing $\hat{q}(B=0)$ in terms of a simple quasi-particle form either $\hat{q}(B=0) = g(T) \times 5.87 T^3$ from Eq. (12) or $\hat{q}(B=0) = g(T) \times \hat{q}_0$ from Eq. (13), $\hat{q}_{\parallel,\perp}(T, B)$ can be expressed as:

$$\begin{aligned}\hat{q}_{\parallel}(T, B) &= \frac{47.5}{\left[16 + \frac{7}{8}12 \sum_{u,d,s} \frac{1}{1 + (\tau_c/\tau_B)^2}\right]} \times \left[g(T) \times 5.87 T^3\right] \\ \text{or} \\ \hat{q}_{\parallel}(T, B) &= \frac{47.5}{\left[16 + \frac{7}{8}12 \sum_{u,d,s} \frac{1}{1 + (\tau_c/\tau_B)^2}\right]} \times \left[g(T) \hat{q}_0\right]\end{aligned}\quad (23)$$

$$\begin{aligned}\hat{q}_{\perp}(T, B) &= \frac{47.5}{\left[16 + \frac{7}{8}12 \sum_{u,d,s} \frac{1}{1 + 4(\tau_c/\tau_B)^2}\right]} \times \left[g(T) \times 5.87 T^3\right] \\ \text{or} \\ \hat{q}_{\perp}(T, B) &= \frac{47.5}{\left[16 + \frac{7}{8}12 \sum_{u,d,s} \frac{1}{1 + 4(\tau_c/\tau_B)^2}\right]} \times \left[g(T) \hat{q}_0\right]\end{aligned}\quad (24)$$

For more rich B -dependent structure, $g(T)$ is replaced by $g(T, B)$. Here, jet transport coefficient for quark jets has parallel and perpendicular components ($\hat{q}_{\parallel, \perp}^q$) which is not expected for gluon jet transport coefficient (\hat{q}^g). Therefore, the final expressions of gluon and quark jets at finite B can be written as:

$$\hat{q}^g(T, B) = g(T, B) \times 5.87 T^3$$

or

$$\hat{q}^g(T, B) = g(T, B) \hat{q}_0 \quad (25)$$

$$\hat{q}_{\parallel}^q(T, B) = \frac{47.5}{\left[16 + \frac{7}{8} 12 \sum_{u,d,s} \frac{1}{1+(\tau_c/\tau_B)^2}\right]} \times \left[g(T, B) \times 5.87 T^3\right]$$

or

$$\hat{q}_{\parallel}^q(T, B) = \frac{47.5}{\left[16 + \frac{7}{8} 12 \sum_{u,d,s} \frac{1}{1+(\tau_c/\tau_B)^2}\right]} \times \left[g(T, B) \hat{q}_0\right] \quad (26)$$

$$\hat{q}_{\perp}^q(T, B) = \frac{47.5}{\left[16 + \frac{7}{8} 12 \sum_{u,d,s} \frac{1}{1+4(\tau_c/\tau_B)^2}\right]} \times \left[g(T, B) \times 5.87 T^3\right]$$

or

$$\hat{q}_{\perp}^q(T, B) = \frac{47.5}{\left[16 + \frac{7}{8} 12 \sum_{u,d,s} \frac{1}{1+4(\tau_c/\tau_B)^2}\right]} \times \left[g(T, B) \hat{q}_0\right] \quad (27)$$

4 Results and discussions

4.1 \hat{q} in absence of magnetic field

First, the quasi-particle based numerical estimation of \hat{q} in absence of magnetic field is calibrated with its standard values available in existing references and then its modification in presence of magnetic field is studied. The temperature dependence of \hat{q}/T^3 is estimated using the quasi-particle model in absence of magnetic field as shown in Fig. 2 and compared with earlier estimations of Refs. [40, 60–67]. In Fig. 2 (left), the red dashed line shows the \hat{q} estimation using Eq. (12) starting from low (hadronic) to high (QGP) temperature taking \hat{q} at the center of cold nuclear matter ($\hat{q}_N \approx 0.02 \text{ GeV}^2/\text{fm}$) as reference point. It represents a crossover type transition in $\hat{q}(T)$ due to the continuous profile of $g(T)$, which carries the information of LQCD thermodynamics. The solid blue line in the left panel of Fig. 2 shows data taken from Ref. [23]. It represents a first-order type transition in \hat{q} owing to the fact that it is constrained by the hadron density ρ_h of the HRG model in hadronic temperature, whereas, for quark temperature range, beyond the transition temperature, jet transport coefficient at the initial time of QGP formation, \hat{q}_0 ($\approx 0.9 \text{ GeV}^2/\text{fm}$) is used. One can find that the estimation of \hat{q}/T^3 in quasi-particle model (solid green line) is comparable to the HRG estimation (solid blue line) in the hadronic temperature range.

The green dash-dotted and solid lines in Fig. 2 (left) show results based on pQCD + HTL approximation [60] for quark jets of initial energy 2 and 10 GeV respectively. It is interesting to observe that the results based on the pQCD + HTL approximation are quite comparable to that obtained from quasi-particle model based on Eq. (12). Therefore, one

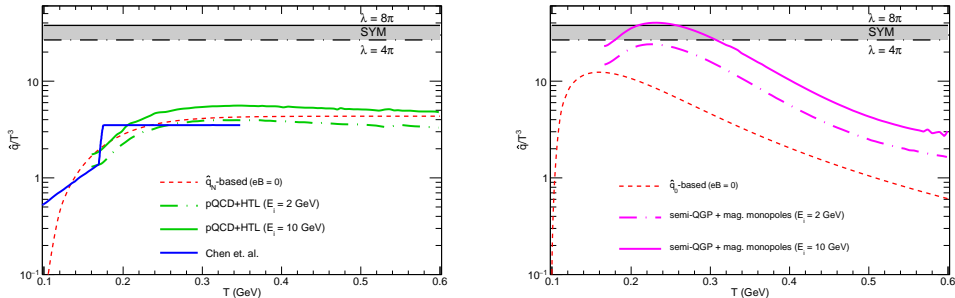


Figure 2: Temperature dependence of \hat{q}/T^3 based on \hat{q}_N and \hat{q}_0 in absence of magnetic field are depicted by the red dashed line in left and right panels respectively. The green (left) and magenta (right) lines represent pQCD + HTL approximations and semi-QGP + magnetic monopoles estimations respectively for quark jet of initial energy $E_i = 2$ GeV (dash-dotted) and 10 GeV (solid) in absence of magnetic field [40]. The blue curve (left) is taken from Chen et al., Ref. [23] to compare with \hat{q}_N based results. Black dash-dotted and solid lines represent \hat{q} of an isotropic $\mathcal{N} = 4$ SYM plasma at zero magnetic field for $\lambda = 4\pi$ and 8π respectively.

may relate the estimation based on \hat{q}_N in the quasi-particle model to a weakly coupled QGP system, as traditionally described by pQCD calculations. In Fig. 2 (right), the red dashed line shows \hat{q} estimation using Eq. (13) starting from high (QGP) to low (hadronic) temperature taking \hat{q} at the initial time of QGP formation ($\hat{q}_0 \approx 0.9$ GeV²/fm) as reference point. Interestingly, \hat{q}/T^3 from Eq. (13) shows a mild peak structure near the transition temperature. Analyzing T dependence of Eq. (12) and Eq. (13), one can recognize $\hat{q} \propto g(T) \times T^3$ and $\hat{q} \propto g(T)$ respectively, so their normalizing function will be $\hat{q}/T^3 \propto g(T)$ and $\hat{q}/T^3 \propto g(T)/T^3$ respectively. It is due to the collective roles of increasing $g(T)$ and decreasing $1/T^3$ that the peak structure is obtained for the latter case.

The magenta dash-dotted and solid lines in Fig. 2 (right) show semi-QGP + magnetic monopoles results [40] for quark jets of initial energy 2 and 10 GeV respectively. The black lines in Fig.2 (right) depict the jet transport coefficient in absence of magnetic field for an isotropic $\mathcal{N} = 4$ SYM plasma of the form [68]:

$$\hat{q}_0 = \frac{\pi^{\frac{3}{2}} \Gamma(\frac{3}{4})}{\Gamma(\frac{5}{4})} \sqrt{\lambda} T^3 \quad (28)$$

where $\sqrt{\lambda} = \sqrt{g_{YM}^2 N_c}$ with g_{YM} denoting the coupling strength of the strongly coupled plasma with color degeneracy factor N_c . The dash-dotted and solid black lines correspond to $\lambda = 4\pi$ and 8π respectively. It is observed that the semi-QGP + magnetic monopoles based results show qualitatively similar behaviour to that obtained from quasi-particle model based on Eq. (13). Both have a peak structure near transition temperatures of their respective models, and their peak strengths are close to the boundary predicted for $\mathcal{N} = 4$ SYM plasma. One may, therefore, relate \hat{q}_0 -based estimation in the quasi-particle model with a strongly coupled QGP system.

It is quite interesting to observe a two-directional aspect of QCD matter by calibrating with existing experimental knowledge of \hat{q} for cold nuclear matter ($\hat{q}_N \approx 0.02$ GeV²/fm) and

for hot QGP ($\hat{q}_0 \approx 0.9 \text{ GeV}^2/\text{fm}$). When one approaches from the hadronic phase to the QGP phase with \hat{q}_N as reference point, the results obtained are close to those of a weakly coupled QGP system. On the other hand, when one approaches from QGP to hadronic phase with \hat{q}_0 as reference point, the results favour a strongly coupled QGP system.

After calibrating the numerical estimations of the two possible simple (quasi-particle model based) expressions with existing values of weakly and strongly coupled QGP systems, the next aim is to see their changes due to finite magnetic field, which is discussed in the next subsection. The main focal point of present work is the relative changes in \hat{q} due to magnetic field, therefore the absolute values of $\hat{q}(B = 0)$ may be considered as a reference point only.

4.2 \hat{q} in presence of finite magnetic field

The temperature dependence of \hat{q}/T^3 in presence of magnetic field taking \hat{q}_N as reference point as described by Eq. (12) and taking \hat{q}_0 as reference point as described by Eq. (13) are shown in left and right panels of Fig. 3 respectively. The solid red lines in top panels of

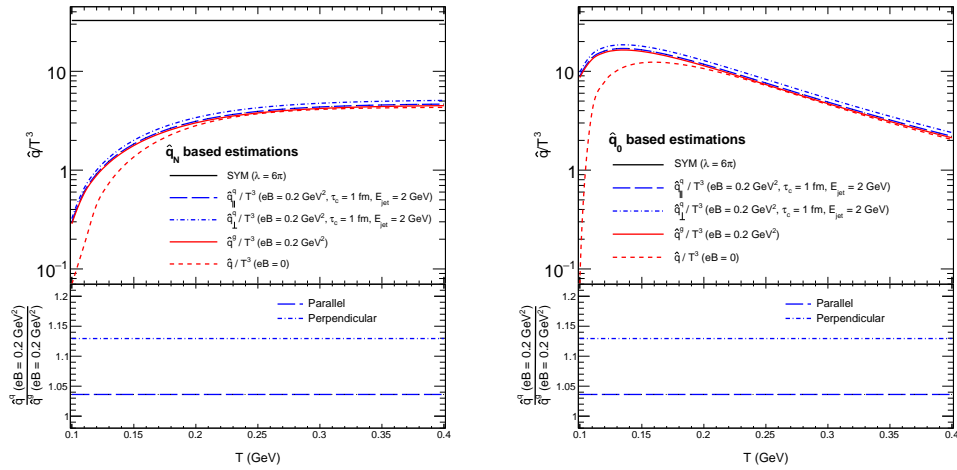


Figure 3: Top panels: Temperature (T in GeV) dependence of $\hat{q}_{\parallel,\perp}^q/T^3$ (blue long dashed and dash-dotted lines) at $eB = 0.2 \text{ GeV}^2$, $\tau_c = 1 \text{ fm}$ are depicted for quark jet of initial energy $E_{jet} = 2 \text{ GeV}$ using Eqs. (22) & (12) (left) and Eqs. (22) & (13) (right). The red solid line shows T dependence of \hat{q}^g/T^3 for gluon jet at $eB = 0.2 \text{ GeV}^2$ obtained using Eq. (12) (left) and Eq. (13) (right). Red dashed lines of both figures represent \hat{q}/T^3 at $eB = 0$ estimated using Eq. (12) (left) and Eq. (13) (right). Black solid line corresponds to an isotropic $\mathcal{N} = 4$ SYM plasma at zero magnetic field for $\lambda = 6\pi$ [Eq. (28)]. Bottom panels: The ratios between $\hat{q}_{\parallel,\perp}^q$ and \hat{q}^g in presence of magnetic field.

Fig. 3 show \hat{q}/T^3 for gluon jets (\hat{q}^g) at finite magnetic field, $eB = 0.2 \text{ GeV}^2$, estimated from Eq. (25). The parallel and perpendicular components of \hat{q}/T^3 at $eB = 0.2 \text{ GeV}^2$ for quark jets of initial energy 2 GeV are shown by long dashed and dash-dotted blue lines respectively. These results are obtained from the parallel (\hat{q}_{\parallel}^q) and perpendicular (\hat{q}_{\perp}^q) expressions, given in Eqs. (26) and (27) respectively. The solid black lines depict the jet transport coefficient

for an isotropic $\mathcal{N} = 4$ SYM plasma at $\lambda = 6\pi$. The dashed red lines representing \hat{q}/T^3 in absence of magnetic field are also shown in top panels of Fig. 3 for reference.

Qualitatively the temperature dependence of \hat{q}/T^3 in presence of magnetic field is found to have similar behaviour to that in absence of magnetic field. At lower temperature, significant enhancement of \hat{q}/T^3 is observed in presence of magnetic field and the enhancement reduces with the increasing temperature for both gluon and quark jets. If one analyzes the detailed anatomy of \hat{q}/T^3 of quark jet, given in Eqs. (26)-(27), then one can identify two sources of B -dependent components. One is B -dependent degeneracy factor, for which jet transport coefficient gets enhanced, and another is the phase space part made of τ_B , for which \hat{q} is further enhanced. However for gluon jets, later component is missing due to their chargeless nature. The bottom panels of Fig. 3 show ratios of parallel and perpendicular components of \hat{q}^q for quark jets to \hat{q}^g for gluon jets in presence of magnetic field. It is interesting to observe that the enhancement in the values of \hat{q} due to presence of magnetic field is about 4% and 13% more for parallel and perpendicular components of quark jets respectively compared to that for gluon jets. So, one can indirectly observe two interesting aspects of QGP at finite magnetic field via jet probe. Former part of quark jet contains magneto-thermodynamics of QCD matter via $g(T, B)$ and its later part is connected with thermodynamical phase shrinking due to cyclotron motion of quark jet. Therefore, the present investigation is hinting at a possibility of difference between jet quenching phenomena for quarks and gluons in presence of magnetic field.

The picture can be understood as follows. During the jet quenching mechanism, two components are involved. One is probe particle, that is either quark or gluon, which will eventually produce a collimated shower of particles, jets. Another is medium, which is assumed to be gluon dominated. Now, in presence of magnetic field, any thermodynamical quantity like gluon density will be modified. This modification is connected with the rich quark-condensate or constituent quark mass profile as a function of T and B . Recent LQCD calculations [32, 33] predicted an inverse magnetic catalysis profile near the transition temperature, for which the transition temperature decreases with increasing magnetic field. This LQCD-based T , B -dependent quark condensate profile will build magneto-thermodynamical phase space of different thermodynamical quantities like entropy density, pressure etc. We have tuned that profile via T , B -dependent degeneracy factor $g(T, B)$. Calculating the corresponding gluon-dominated medium density at finite B using this $g(T, B)$, we have incorporated B -dependent information of medium into jet transport coefficient \hat{q} as it is proportionally connected to the density of the medium.

Next, let us discuss the B -dependent information of probe particle. For gluon jet probe, no modification is possible but for quark jet, modification comes from the Lorentz force. A mild bending of quark jet propagation is expected due to its cyclotron motion, quantified through τ_B . This B -dependent information has been indirectly incorporated in the present work through the B -dependent phase space factor of shear viscosity to entropy density ratio.

This impact of magnetic field on \hat{q} might be challenging to observe experimentally, however, one can perform a comparative study by measuring nuclear suppression factor R_{AA} separately for quark and gluon initiated jets in central (where eB is expected to be zero) and non-central (where eB is expected to be non-zero) heavy-ion collisions. The quarks being charged will be affected more than gluons in presence of magnetic field. Therefore, if the experiment can be designed for these two separate measurements, the difference between two measurements can be attributed to the B dependence of jet transport coefficient.

4.3 Comparison to AdS/CFT Correspondence

The jet transport coefficient \hat{q} for the strongly coupled QCD plasma in presence of a magnetic field has also been computed directly using the non-perturbative toolbox of the AdS/CFT correspondence [69–75]. It has been shown that compared to the pQCD estimation, the mag-

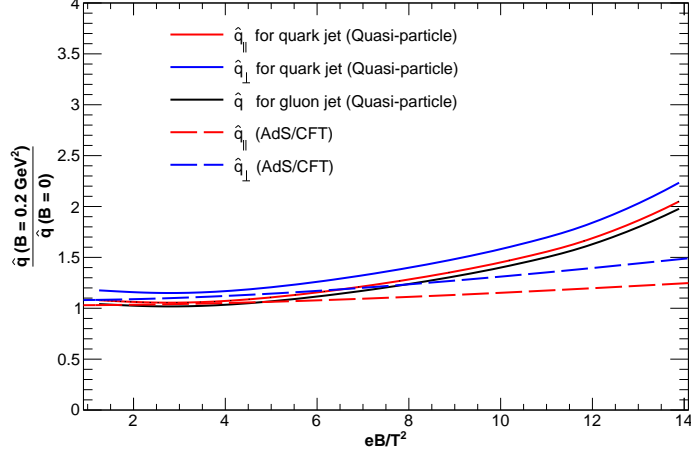


Figure 4: Comparison of the results for the ratio of $\hat{q}(B)$ to $\hat{q}(B = 0)$ obtained from the quasi-particle like approach against AdS/CFT correspondence for $eB = 0.2 \text{ GeV}^2$ and $\tau_c = 1 \text{ fm}$. The results for the quasi-particle approach are shown as solid lines, and those from AdS/CFT correspondence [75] are shown by the dashed lines.

nitude of $\hat{q}(B = 0)$ calculated via the AdS/CFT correspondence is closer to that extracted from RHIC data [76, 77]. If the magnetic field is along the z -direction, the parton that forms the jet while traversing through the medium can suffer a momentum broadening either along or transverse to the magnetic field direction, giving rise to three different components of jet transport coefficient: $\hat{q}_{\parallel(\perp)}$, $\hat{q}_{\perp(\parallel)}$ and $\hat{q}_{\perp(\perp)}$, where $\hat{q}_{\parallel} \equiv \hat{q}_{\parallel(\perp)}$ and $\hat{q}_{\perp} \equiv \hat{q}_{\perp(\parallel)} + \hat{q}_{\perp(\perp)}$. In this notation, the first and second symbols denote the direction of the moving parton and the direction in which the momentum broadening of the jet occurs respectively with respect to the magnetic field direction.

Fig. (4) shows an interesting comparison for the ratio $\hat{q}(B)/\hat{q}(B = 0)$ obtained from quasi-particle model using Eq. (23) against the AdS/CFT correspondence results for values of eB/T^2 up to 14. Both find $\hat{q}_{\perp} > \hat{q}_{\parallel}$ and support enhancing trend of jet transport coefficient in presence of magnetic field, however, a quantitative difference is observed between them. One of the possible reasons might be that the current estimation of \hat{q} from quasi-particle model has not adopted the quantum aspect of the magnetic field, where the phase space will be proportional to eB due to Landau quantization. In that case, one might get a proportional eB dependence as one grossly notice for the AdS/CFT correspondence results. In future, one can extend the present work in that direction.

5 Summary

In summary, we presented the estimation of jet transport coefficient, \hat{q} using a simple quasi-particle model where a temperature-dependent degeneracy factor $g(T)$ of partons is considered whose parameters are obtained by fitting the entropy density of lattice quantum chromodynamics. Although we are unable to properly fit the other thermodynamical quantities such as energy density, pressure with the same set of parameters of $g(T)$, however, this model provides a simple and easy-dealing tool which is consistent with QCD thermodynamics within a given range of temperature for the estimation of jet transport coefficient. Using the parametric degeneracy factor, we have estimated the temperature-dependent gluon density to obtain $\hat{q}(T)$ from hadronic to QGP phase by restricting low- and high-temperature values of \hat{q} by their experimental values. During the restriction by low-temperature cold nuclear matter data, temperature-dependent $\hat{q}(T)$ from hadronic to QGP phase becomes quite close to the HTL or perturbative QCD results, which indicate transportation of jet in weakly interacting gas. On the other hand, $\hat{q}(T)$ estimation from QGP to hadronic phase is qualitatively similar to earlier estimates based on semi-QGP + magnetic monopoles, which correspond to a strongly interacting liquid picture.

After calibrating our quasi-particle estimations with earlier results, we have gone through their finite magnetic field extensions. The effect of finite magnetic field is introduced in the model by replacing the temperature-dependent degeneracy factor $g(T)$ with temperature and magnetic field-dependent degeneracy factor $g(T, B)$ whose parameters are obtained by fitting the magneto-thermodynamical data of lattice quantum chromodynamics. The jet transport coefficient $\hat{q}(T, B)$ is calculated for both quark- and gluon-initiated jets. For quark jets, it splits into parallel and perpendicular components carrying magnetic field dependence from two sources: the field-dependent degeneracy factor and the phase space part guided from the shear viscosity to entropy density ratio. The value of \hat{q} is found to be enhanced due to the collective role of these two sources for quark jets and in case of gluon jets, only the field-dependent degeneracy factor comes into play. The \hat{q} for gluon jets and both the parallel and perpendicular components for quark jets show a significant enhancement at low temperature which gradually decreases towards high temperature. A similar enhancement of jet transport coefficients at finite magnetic field is also observed in the AdS/CFT correspondence calculations. Quasi-particle model results can provide additional information towards our current understanding and phenomenology of jet quenching in presence of the magnetic field.

It would be very interesting to experimentally perform a comparative study by measuring nuclear suppression factor R_{AA} separately for quark and gluon initiated jets in central (where eB is expected to be zero) and non-central (where eB is expected to be non-zero) heavy-ion collisions as quarks being electrically charged are expected to experience the effect of the magnetic field more compared to the electrically neutral gluons.

Acknowledgement: The authors acknowledge following members of [TPRC-IITBH](#) who previously worked on quasi-particle picture [29, 54]: Sarthak Satapathy, Jayanta Dey, Anki Anand, Ranjesh Kumar, Ankita Mishra and Prasant Murmu. D. Banerjee acknowledges the Inspire Fellowship research grant [DST/INSPIRE Fellowship/2018/IF180285]. A. Modak and P. Das acknowledge the Institutional Fellowship research grant of Bose Institute. Significant part of computation for this work was carried out using the computing server facility at CAPSS, Bose Institute, Kolkata.

References

- [1] M. Connors, C. Nattrass, R. Reed, and S. Salur, “Jet measurements in heavy ion physics,” *Rev. Mod. Phys.* **90** (2018) 025005, [arXiv:1705.01974 \[nucl-ex\]](#).
- [2] I. Y. Aref’eva, “Formation time of quark–gluon plasma in heavy-ion collisions in the holographic shock wave model,” *Teor. Mat. Fiz.* **184** no. 3, (2015) 398–417, [arXiv:1503.02185 \[hep-th\]](#).
- [3] R. Chatterjee and D. K. Srivastava, “Formation Time of QGP from Thermal Photon Elliptic Flow,” *Nucl. Phys. A* **830** (2009) 503C–506C, [arXiv:0907.3548 \[nucl-th\]](#).
- [4] M. Gyulassy and M. Plumer, “Jet Quenching in Dense Matter,” *Phys. Lett. B* **243** (1990) 432–438.
- [5] X.-N. Wang and M. Gyulassy, “Gluon shadowing and jet quenching in A + A collisions at $\sqrt{s_{NN}} = 200$ GeV,” *Phys. Rev. Lett.* **68** (1992) 1480–1483.
- [6] A. Majumder and M. Van Leeuwen, “The Theory and Phenomenology of Perturbative QCD Based Jet Quenching,” *Prog. Part. Nucl. Phys.* **66** (2011) 41–92, [arXiv:1002.2206 \[hep-ph\]](#).
- [7] JET, K. M. Burke *et al.*, “Extracting the jet transport coefficient from jet quenching in high-energy heavy-ion collisions,” *Phys. Rev. C* **90** no. 1, (2014) 014909, [arXiv:1312.5003 \[nucl-th\]](#).
- [8] NA49, A. Laszlo, “Nuclear modification at $\sqrt{s_{NN}} = 17.3$ GeV, measured at NA49,” *Indian J. Phys.* **85** (2011) 787–791, [arXiv:0805.4771 \[nucl-ex\]](#).
- [9] PHENIX Collaboration, A. Adare *et al.*, “Transverse momentum dependence of η meson suppression in Au + Au collisions at $\sqrt{s_{NN}} = 200$ GeV,” *Phys. Rev. C* **82** (Jul, 2010) 011902. <https://link.aps.org/doi/10.1103/PhysRevC.82.011902>.
- [10] CMS, S. Chatrchyan *et al.*, “Study of high-pT charged particle suppression in PbPb compared to pp collisions at $\sqrt{s_{NN}} = 2.76$ TeV,” *Eur. Phys. J. C* **72** (2012) 1945, [arXiv:1202.2554 \[nucl-ex\]](#).
- [11] CMS, V. Khachatryan *et al.*, “Measurement of inclusive jet production and nuclear modifications in pPb collisions at $\sqrt{s_{NN}} = 5.02$ TeV,” *Eur. Phys. J. C* **76** no. 7, (2016) 372, [arXiv:1601.02001 \[nucl-ex\]](#).
- [12] ALICE, B. Abelev *et al.*, “Measurement of charged jet suppression in Pb-Pb collisions at $\sqrt{s_{NN}} = 2.76$ TeV,” *JHEP* **03** (2014) 013, [arXiv:1311.0633 \[nucl-ex\]](#).
- [13] R. Baier, Y. L. Dokshitzer, A. H. Mueller, S. Peigne, and D. Schiff, “Radiative energy loss and p(T) broadening of high-energy partons in nuclei,” *Nucl. Phys. B* **484** (1997) 265–282, [arXiv:hep-ph/9608322](#).
- [14] B. G. Zakharov, “Radiative energy loss of high-energy quarks in finite size nuclear matter and quark - gluon plasma,” *JETP Lett.* **65** (1997) 615–620, [arXiv:hep-ph/9704255](#).
- [15] M. Gyulassy, P. Levai, and I. Vitev, “Reaction operator approach to nonAbelian energy loss,” *Nucl. Phys. B* **594** (2001) 371–419, [arXiv:nucl-th/0006010](#).

- [16] I. Vitev and M. Gyulassy, “High- p_T Tomography of $d + Au$ and $Au + Au$ at SPS, RHIC, and LHC,” *Phys. Rev. Lett.* **89** (Dec, 2002) 252301. <https://link.aps.org/doi/10.1103/PhysRevLett.89.252301>.
- [17] A. Buzzatti and M. Gyulassy, “Jet Flavor Tomography of Quark Gluon Plasmas at RHIC and LHC,” *Phys. Rev. Lett.* **108** (Jan, 2012) 022301. <https://link.aps.org/doi/10.1103/PhysRevLett.108.022301>.
- [18] B. Schenke, C. Gale, and S. Jeon, “MARTINI: An event generator for relativistic heavy-ion collisions,” *Phys. Rev. C* **80** (Nov, 2009) 054913. <https://link.aps.org/doi/10.1103/PhysRevC.80.054913>.
- [19] G.-Y. Qin, J. Ruppert, C. Gale, S. Jeon, G. D. Moore, and M. G. Mustafa, “Radiative and Collisional Jet Energy Loss in the Quark-Gluon Plasma at the BNL Relativistic Heavy Ion Collider,” *Phys. Rev. Lett.* **100** (Feb, 2008) 072301. <https://link.aps.org/doi/10.1103/PhysRevLett.100.072301>.
- [20] A. Majumder, “Hard collinear gluon radiation and multiple scattering in a medium,” *Phys. Rev. D* **85** (Jan, 2012) 014023. <https://link.aps.org/doi/10.1103/PhysRevD.85.014023>.
- [21] X. Guo and X.-N. Wang, “Multiple Scattering, Parton Energy Loss, and Modified Fragmentation Functions in Deeply Inelastic eA Scattering,” *Phys. Rev. Lett.* **85** (Oct, 2000) 3591–3594. <https://link.aps.org/doi/10.1103/PhysRevLett.85.3591>.
- [22] X.-N. Wang and X. Guo, “Multiple parton scattering in nuclei: parton energy loss,” *Nuclear Physics A* **696** no. 3, (2001) 788–832. <https://www.sciencedirect.com/science/article/pii/S0375947401011307>.
- [23] X.-F. Chen, C. Greiner, E. Wang, X.-N. Wang, and Z. Xu, “Bulk matter evolution and extraction of jet transport parameters in heavy-ion collisions at energies available at the BNL Relativistic Heavy Ion Collider (RHIC),” *Phys. Rev. C* **81** (Jun, 2010) 064908. <https://link.aps.org/doi/10.1103/PhysRevC.81.064908>.
- [24] PHENIX Collaboration, A. Adare *et al.*, “Suppression Pattern of Neutral Pions at High Transverse Momentum in $Au + Au$ Collisions at $\sqrt{s_{NN}} = 200$ GeV and Constraints on Medium Transport Coefficients,” *Phys. Rev. Lett.* **101** (Dec, 2008) 232301. <https://link.aps.org/doi/10.1103/PhysRevLett.101.232301>.
- [25] PHENIX Collaboration, A. Adare *et al.*, “Neutral pion production with respect to centrality and reaction plane in $Au+Au$ collisions at $\sqrt{s_{NN}} = 200$ GeV,” *Phys. Rev. C* **87** (Mar, 2013) 034911. <https://link.aps.org/doi/10.1103/PhysRevC.87.034911>.
- [26] ALICE, B. Abelev *et al.*, “Centrality Dependence of Charged Particle Production at Large Transverse Momentum in Pb–Pb Collisions at $\sqrt{s_{NN}} = 2.76$ TeV,” *Phys. Lett. B* **720** (2013) 52–62, [arXiv:1208.2711](https://arxiv.org/abs/1208.2711) [hep-ex].
- [27] CMS, S. Chatrchyan *et al.*, “Study of high-pT charged particle suppression in PbPb compared to pp collisions at $\sqrt{s_{NN}} = 2.76$ TeV,” *Eur. Phys. J. C* **72** (2012) 1945, [arXiv:1202.2554](https://arxiv.org/abs/1202.2554) [nucl-ex].

- [28] K. Tuchin, “Particle production in strong electromagnetic fields in relativistic heavy-ion collisions,” *Adv. High Energy Phys.* **2013** (2013) 490495, [arXiv:1301.0099 \[hep-ph\]](#).
- [29] S. Satapathy, S. Paul, A. Anand, R. Kumar, and S. Ghosh, “From Non-interacting to Interacting Picture of Thermodynamics and Transport Coefficients for Quark Gluon Plasma,” *J. Phys. G* **47** no. 4, (2020) 045201, [arXiv:1908.04330 \[hep-ph\]](#).
- [30] S. Borsányi, Z. Fodor, C. Hoelbling, S. D. Katz, S. Krieg, and K. K. Szabó, “Full result for the QCD equation of state with 2+1 flavors,” *Physics Letters B* **730** (2014) 99–104. <https://www.sciencedirect.com/science/article/pii/S0370269314000197>.
- [31] HotQCD Collaboration, A. Bazavov, T. Bhattacharya, C. DeTar, H.-T. Ding, S. Gottlieb, R. Gupta, P. Hegde, U. M. Heller, F. Karsch, E. Laermann, L. Levkova, S. Mukherjee, P. Petreczky, C. Schmidt, C. Schroeder, R. A. Soltz, W. Soeldner, R. Sugar, M. Wagner, and P. Vranas, “Equation of state in $(2 + 1)$ -flavor QCD,” *Phys. Rev. D* **90** (Nov, 2014) 094503. <https://link.aps.org/doi/10.1103/PhysRevD.90.094503>.
- [32] G. S. Bali, F. Bruckmann, G. Endrődi, Z. Fodor, S. D. Katz, and A. Schäfer, “QCD quark condensate in external magnetic fields,” *Phys. Rev. D* **86** (Oct, 2012) 071502. <https://link.aps.org/doi/10.1103/PhysRevD.86.071502>.
- [33] G. S. Bali, F. Bruckmann, G. Endrődi, S. D. Katz, and A. Schäfer, “The QCD equation of state in background magnetic fields,” *JHEP* **08** (2014) 177, [arXiv:1406.0269 \[hep-lat\]](#).
- [34] X. Li, W.-j. Fu, and Y.-x. Liu, “Thermodynamics of 2 + 1 flavor Polyakov-loop quark-meson model under external magnetic field,” *Phys. Rev. D* **99** (Apr, 2019) 074029. <https://link.aps.org/doi/10.1103/PhysRevD.99.074029>.
- [35] A. N. Tawfik, A. M. Diab, and M. T. Hussein, “Quark–hadron phase structure, thermodynamics, and magnetization of QCD matter,” *J. Phys. G* **45** no. 5, (2018) 055008, [arXiv:1604.08174 \[hep-lat\]](#).
- [36] A. N. Tawfik, A. M. Diab, N. Ezzelarab, and A. G. Shalaby, “QCD thermodynamics and magnetization in nonzero magnetic field,” *Adv. High Energy Phys.* **2016** (2016) 1381479, [arXiv:1604.00043 \[hep-ph\]](#).
- [37] R. L. S. Farias, V. S. Timoteo, S. S. Avancini, M. B. Pinto, and G. Krein, “Thermo-magnetic effects in quark matter: Nambu–Jona-Lasinio model constrained by lattice QCD,” *Eur. Phys. J. A* **53** no. 5, (2017) 101, [arXiv:1603.03847 \[hep-ph\]](#).
- [38] A. Majumder, B. Müller, and X.-N. Wang, “Small Shear Viscosity of a Quark-Gluon Plasma Implies Strong Jet Quenching,” *Phys. Rev. Lett.* **99** (Nov, 2007) 192301. <https://link.aps.org/doi/10.1103/PhysRevLett.99.192301>.
- [39] J. Casalderrey-Solana and X.-N. Wang, “Energy dependence of jet transport parameter and parton saturation in quark-gluon plasma,” *Phys. Rev. C* **77** (Feb, 2008) 024902. <https://link.aps.org/doi/10.1103/PhysRevC.77.024902>.

- [40] J. Xu, J. Liao, and M. Gyulassy, “Consistency of Perfect Fluidity and Jet Quenching in Semi-Quark-Gluon Monopole Plasmas,” *Chinese Physics Letters* **32** no. 9, (Aug, 2015) 092501. <https://doi.org/10.1088/0256-307x/32/9/092501>.
- [41] J. Xu, J. Liao, and M. Gyulassy, “Bridging Soft-Hard Transport Properties of Quark-Gluon Plasmas with CUJET3.0,” *JHEP* **02** (2016) 169, [arXiv:1508.00552](https://arxiv.org/abs/1508.00552) [hep-ph].
- [42] E. Shuryak, “Strongly coupled quark-gluon plasma in heavy ion collisions,” *Rev. Mod. Phys.* **89** (Jul, 2017) 035001. <https://link.aps.org/doi/10.1103/RevModPhys.89.035001>.
- [43] A. Ayala, I. Dominguez, J. Jalilian-Marian, and M. E. Tejeda-Yeomans, “Relating \hat{q} , η/s , and ΔE in an expanding quark-gluon plasma,” *Phys. Rev. C* **94** (Aug, 2016) 024913. <https://link.aps.org/doi/10.1103/PhysRevC.94.024913>.
- [44] HERMES, A. Airapetian *et al.*, “Hadronization in semi-inclusive deep-inelastic scattering on nuclei,” *Nucl. Phys. B* **780** (2007) 1–27, [arXiv:0704.3270](https://arxiv.org/abs/0704.3270) [hep-ex].
- [45] W.-T. Deng and X.-N. Wang, “Multiple parton scattering in nuclei: Modified Dokshitzer-Gribov-Lipatov-Altarelli-Parisi (DGLAP) evolution for fragmentation functions,” *Phys. Rev. C* **81** (Feb, 2010) 024902. <https://link.aps.org/doi/10.1103/PhysRevC.81.024902>.
- [46] E. Lifshitz and P. L.P., *Physical Kinetics*. Elsevier India, 1981.
- [47] X.-G. Huang, M. Huang, D. H. Rischke, and A. Sedrakian, “Anisotropic hydrodynamics, bulk viscosities, and r -modes of strange quark stars with strong magnetic fields,” *Phys. Rev. D* **81** (Feb, 2010) 045015. <https://link.aps.org/doi/10.1103/PhysRevD.81.045015>.
- [48] X.-G. Huang, A. Sedrakian, and D. H. Rischke, “Kubo formulae for relativistic fluids in strong magnetic fields,” *Annals Phys.* **326** (2011) 3075–3094, [arXiv:1108.0602](https://arxiv.org/abs/1108.0602) [astro-ph.HE].
- [49] K. Tuchin, “On viscous flow and azimuthal anisotropy of quark-gluon plasma in strong magnetic field,” *J. Phys. G* **39** (2012) 025010, [arXiv:1108.4394](https://arxiv.org/abs/1108.4394) [nucl-th].
- [50] S. Li and H.-U. Yee, “Shear viscosity of the quark-gluon plasma in a weak magnetic field in perturbative QCD: Leading log,” *Phys. Rev. D* **97** no. 5, (2018) 056024, [arXiv:1707.00795](https://arxiv.org/abs/1707.00795) [hep-ph].
- [51] P. Mohanty, A. Dash, and V. Roy, “One particle distribution function and shear viscosity in magnetic field: a relaxation time approach,” *Eur. Phys. J. A* **55** (2019) 35, [arXiv:1804.01788](https://arxiv.org/abs/1804.01788) [nucl-th].
- [52] S. Ghosh, B. Chatterjee, P. Mohanty, A. Mukharjee, and H. Mishra, “Impact of magnetic field on shear viscosity of quark matter in Nambu–Jona-Lasinio model,” *Phys. Rev. D* **100** no. 3, (2019) 034024, [arXiv:1804.00812](https://arxiv.org/abs/1804.00812) [hep-ph].
- [53] S.-i. Nam and C.-W. Kao, “Shear viscosity of quark matter at finite temperature under an external magnetic field,” *Phys. Rev. D* **87** (Jun, 2013) 114003. <https://link.aps.org/doi/10.1103/PhysRevD.87.114003>.

- [54] J. Dey, S. Satapathy, A. Mishra, S. Paul, and S. Ghosh, “From noninteracting to interacting picture of quark–gluon plasma in the presence of a magnetic field and its fluid property,” *Int. J. Mod. Phys. E* **30** no. 06, (2021) 2150044, [arXiv:1908.04335 \[hep-ph\]](#).
- [55] A. Dash, S. Samanta, J. Dey, U. Gangopadhyaya, S. Ghosh, and V. Roy, “Anisotropic transport properties of a hadron resonance gas in a magnetic field,” *Phys. Rev. D* **102** no. 1, (2020) 016016, [arXiv:2002.08781 \[nucl-th\]](#).
- [56] A. Das, H. Mishra, and R. K. Mohapatra, “Transport coefficients of hot and dense hadron gas in a magnetic field: A relaxation time approach,” *Phys. Rev. D* **100** (Dec, 2019) 114004. <https://link.aps.org/doi/10.1103/PhysRevD.100.114004>.
- [57] G. S. Denicol, X.-G. Huang, E. Molnár, G. M. Monteiro, H. Niemi, J. Noronha, D. H. Rischke, and Q. Wang, “Nonresistive dissipative magnetohydrodynamics from the Boltzmann equation in the 14-moment approximation,” *Phys. Rev. D* **98** (Oct, 2018) 076009. <https://link.aps.org/doi/10.1103/PhysRevD.98.076009>.
- [58] Z. Chen, C. Greiner, A. Huang, and Z. Xu, “Calculation of anisotropic transport coefficients for an ultrarelativistic Boltzmann gas in a magnetic field within a kinetic approach,” *Phys. Rev. D* **101** (Mar, 2020) 056020. <https://link.aps.org/doi/10.1103/PhysRevD.101.056020>.
- [59] J. Dey, S. Satapathy, P. Murmu, and S. Ghosh, “Shear viscosity and electrical conductivity of the relativistic fluid in the presence of a magnetic field: A massless case,” *Pramana* **95** no. 3, (2021) 125, [arXiv:1907.11164 \[hep-ph\]](#).
- [60] J. Xu, A. Buzzatti, and M. Gyulassy, “Azimuthal jet flavor tomography with CUJET2.0 of nuclear collisions at RHIC and LHC,” *JHEP* **08** (2014) 063, [arXiv:1402.2956 \[hep-ph\]](#).
- [61] Y. Hidaka and R. D. Pisarski, “Suppression of the shear viscosity in a “semi”-quark-gluon plasma,” *Phys. Rev. D* **78** (Oct, 2008) 071501. <https://link.aps.org/doi/10.1103/PhysRevD.78.071501>.
- [62] Y. Hidaka and R. D. Pisarski, “Small shear viscosity in the semiquark gluon plasma,” *Phys. Rev. D* **81** (Apr, 2010) 076002. <https://link.aps.org/doi/10.1103/PhysRevD.81.076002>.
- [63] A. Dumitru, Y. Guo, Y. Hidaka, C. P. K. Altes, and R. D. Pisarski, “How wide is the transition to deconfinement?,” *Phys. Rev. D* **83** (Feb, 2011) 034022. <https://link.aps.org/doi/10.1103/PhysRevD.83.034022>.
- [64] S. Lin, R. D. Pisarski, and V. V. Skokov, “Collisional energy loss above the critical temperature in QCD,” *Physics Letters B* **730** (2014) 236–242. <https://www.sciencedirect.com/science/article/pii/S0370269314000653>.
- [65] J. Liao and E. Shuryak, “Strongly coupled plasma with electric and magnetic charges,” *Phys. Rev. C* **75** (May, 2007) 054907. <https://link.aps.org/doi/10.1103/PhysRevC.75.054907>.

- [66] J. Liao and E. Shuryak, “The Magnetic Component of Quark-Gluon Plasma is also a Liquid,” *Phys. Rev. Lett.* **101** (Oct, 2008) 162302.
<https://link.aps.org/doi/10.1103/PhysRevLett.101.162302>.
- [67] J. Liao and E. Shuryak, “Effect of Light Fermions on the Confinement Transition in QCD-Like Theories,” *Phys. Rev. Lett.* **109** (Oct, 2012) 152001.
<https://link.aps.org/doi/10.1103/PhysRevLett.109.152001>.
- [68] H. Liu, K. Rajagopal, and U. A. Wiedemann, “Calculating the jet quenching parameter from AdS/CFT,” *Phys. Rev. Lett.* **97** (2006) 182301,
[arXiv:hep-ph/0605178](https://arxiv.org/abs/hep-ph/0605178).
- [69] J. M. Maldacena, “The Large N limit of superconformal field theories and supergravity,” *Adv. Theor. Math. Phys.* **2** (1998) 231–252, [arXiv:hep-th/9711200](https://arxiv.org/abs/hep-th/9711200).
- [70] S. S. Gubser, I. R. Klebanov, and A. M. Polyakov, “Gauge theory correlators from noncritical string theory,” *Phys. Lett. B* **428** (1998) 105–114, [arXiv:hep-th/9802109](https://arxiv.org/abs/hep-th/9802109).
- [71] O. Aharony, S. S. Gubser, J. M. Maldacena, H. Ooguri, and Y. Oz, “Large N field theories, string theory and gravity,” *Phys. Rept.* **323** (2000) 183–386,
[arXiv:hep-th/9905111](https://arxiv.org/abs/hep-th/9905111).
- [72] S. Li, K. A. Mamo, and H.-U. Yee, “Jet quenching parameter of the quark-gluon plasma in a strong magnetic field: Perturbative QCD and AdS/CFT correspondence,” *Phys. Rev. D* **94** (Oct, 2016) 085016.
<https://link.aps.org/doi/10.1103/PhysRevD.94.085016>.
- [73] Z.-q. Zhang and K. Ma, “The effect of magnetic field on jet quenching parameter,” *Eur. Phys. J. C* **78** no. 7, (2018) 532.
- [74] K. A. Mamo, “Inverse magnetic catalysis in holographic models of QCD,” *JHEP* **05** (2015) 121, [arXiv:1501.03262](https://arxiv.org/abs/1501.03262) [[hep-th](#)].
- [75] R. Rougemont, “Jet quenching parameters in strongly coupled anisotropic plasmas in the presence of magnetic fields,” *Phys. Rev. D* **102** no. 3, (2020) 034009,
[arXiv:2002.06725](https://arxiv.org/abs/2002.06725) [[hep-ph](#)].
- [76] K. J. Eskola, H. Honkanen, C. A. Salgado, and U. A. Wiedemann, “The Fragility of high-p(T) hadron spectra as a hard probe,” *Nucl. Phys. A* **747** (2005) 511–529,
[arXiv:hep-ph/0406319](https://arxiv.org/abs/hep-ph/0406319).
- [77] A. Dainese, C. Loizides, and G. Paic, “Leading-particle suppression in high energy nucleus-nucleus collisions,” *Eur. Phys. J. C* **38** (2005) 461–474,
[arXiv:hep-ph/0406201](https://arxiv.org/abs/hep-ph/0406201).